coatings

MDPI

Article

A Durable Nano-SiO_2-TiO_2/Dodecyltrimethoxysilane Superhydrophobic Coating for Stone Protection

Meiman Peng [1,2,3], Liqin Wang [1,2,*], Lang Guo [3], Jinyi Guo [3], Liping Zheng [3,4], Fuwei Yang [3], Zhuang Ma [5] and Xing Zhao [3,*]

1 China-Central Asia "the Belt and Road" Joint Laboratory on Human and Environment Research, Xi'an 710127, China
2 Key Laboratory of Cultural Heritage Research and Conservation, Northwest University, Ministry of Education, Xi'an 710127, China
3 School of Cultural Heritage, Northwest University, Xi'an 710127, China
4 School of History and Society, Chongqing Normal University, Chongqing 401331, China
5 Leibniz-Institut für Katalyse e.V., Albert-Einstein-Str. 29a, D-18059 Rostock, Germany
* Correspondence: wangliqinnwuedu@163.com (L.W.); zhaoxing@nwu.edu.cn (X.Z.)

Abstract: Water can trigger freeze–thaw cycles, acid rain corrosion, and microbial colonisation, all of which destroy stone. Water is one of the most influential factors in the destruction of outdoor stone heritage. Therefore, materials with excellent hydrophobic properties and durability are urgently required to effectively retard long-term stone weathering. In this study, two nanoparticles, TiO_2 and SiO_2, were used to modify dodecyltrimethoxysilane (DTMS), a waterproof coating commonly used for stone heritage protection, to fabricate nanocomposite superhydrophobic coatings. The micromorphology, water repellence (water contact angle and capillary water absorption), suitability to protect stone heritage (color change and water vapor permeability), and durability (thermal, light, and chemical stability) of DTMS and nanocomposite coatings were evaluated. The scanning electron microscope (SEM) images revealed that adding 0.5% (*w*/*w*) SiO_2 produced nanoscale roughness on the sandstone surface, leading to superhydrophobicity. The results of ultraviolet -visible (UV–Vis) spectrophotometer showed that adding 0.01% TiO_2 shielded more than 90% of UV light but accelerated the decrease in the contact angle under UVA irradiation. The addition of SiO_2 was able to avoid the detrimental effect of TiO_2 under UV light. The thermogravimetric analysis (TGA) results showed that both SiO_2 and TiO_2 nanoparticles improved the thermal stability of the coatings. In particular, the fabricated nanocomposite coating, SiO_2 and TiO_2 co-modified DTMS, had excellent water repellence, low color change and outstanding durability, and retained about 85% of the water vapor permeability of the stone, showing promise for stone protection.

Keywords: stone protection; SiO_2 nanoparticle; TiO_2 nanoparticle; superhydrophobic coatings; durability; dodecyltrimethoxysilane

check for updates

Citation: Peng, M.; Wang, L.; Guo, L.; Guo, J.; Zheng, L.; Yang, F.; Ma, Z.; Zhao, X. A Durable Nano-SiO_2-TiO_2/Dodecyltrimethoxysilane Superhydrophobic Coating for Stone Protection. *Coatings* **2022**, *12*, 1397. https://doi.org/10.3390/coatings12101397

Academic Editor: Ioannis Karapanagiotis

Received: 30 August 2022
Accepted: 23 September 2022
Published: 25 September 2022

Publisher's Note: MDPI stays neutral with regard to jurisdictional claims in published maps and institutional affiliations.

Copyright: © 2022 by the authors. Licensee MDPI, Basel, Switzerland. This article is an open access article distributed under the terms and conditions of the Creative Commons Attribution (CC BY) license (https://creativecommons.org/licenses/by/4.0/).

1. Introduction

Sandstone, which has a porous structure, is an important component of stone heritage worldwide [1–5]. Outdoor stone heritage is weathered by temperature, humidity, light, polluting gases, etc., with water being the dominant factor influencing weathering. Stones are damaged by dry–wet cycles, freeze–thaw cycles, salt, and biodeterioration because of the presence of water. Controlling this single factor, water, may effectively inhibit damage to stone heritage and its associated components [6].

Fluoropolymers [7,8], siloxane coatings [9], and acrylic polymers [10] are the surface materials most studied and applied to protect stone. Due to their low surface energy, these organic coatings are hydrophobic. Hydrophobic materials, having a static contact angle larger than 150° and low contact angle hysteresis (usually a roll-off angle of less than 10°), are generally referred to as superhydrophobic materials. The water-repellence

ability of superhydrophobic materials enables them to effectively reduce the effect of water erosion, and the low roll-off angle of the surfaces effectively decreases the deposition of contaminants and microorganisms [11], showing potential for the protection of stone artefacts. Obtaining superhydrophobicity requires substances with appropriate roughness and low surface energy [12–14]. A nanocomposite coating, usually prepared with organic coatings and nanoparticles, is currently one of the most used superhydrophobic materials, where the organic component has low surface energy and the nanoparticles provide a rough structure.

Silicones are widely used, low-surface-energy substances that are chemically stabile because of the high-strength Si–O bond. For example, dodecyltrimethoxysilane (DTMS) has been used for alloy anticorrosion [15,16], fabric waterproofing [17], and the protection of historic buildings [18,19] and sandstone [20]. In China, DTMS has been used as a water-repellent coating for the stone artefacts of the Qianling tomb, Maoling tomb, Banpo site, Big Wild Goose Pagoda in Shaanxi Province [21], and Goguryeo site in Jilin Province [22]. Silicones, specifically DTMS, can feasibly be used for conserving stone artefacts. However, its light resistance is poor. After 800 h of UVB irradiation, the water contact angle of a stone surface dropped to 0° [23]. Furthermore, its waterproofing and durability need to be enhanced.

Nanomaterials had initial applications in heritage conservation [24,25]. Organic coatings and nanoparticles are combined to prepare nanocomposite organic coatings with excellent properties. The introduction of nanomaterials may improve the properties of organic coatings, such as their water absorption, thermo–mechanical properties, substrate adhesion, UV and chemical stability, wear resistance [26], and self-cleaning [27], which is expected to improve the durability and water repellence of DTMS, thus further expanding the application of silicones in the field of cultural heritage.

Some researchers have studied the use of single-nanoparticle-modified coatings for the protection of stone artefacts. SiO_2 and TiO_2 nanoparticles are two of the nanoparticles most used for nanocomposite organic coatings to protect cultural heritage [28]. Facia [29] added SiO_2 nanoparticles to siloxane, simply producing superhydrophobic nanocomposite coatings in situ on a sandstone building substrate. TiO_2 nanoparticles [30] were also used to fabricate superhydrophobic nanocomposite coatings, giving photo-catalytic activity and self-cleaning properties [31]. Nano-Al_2O_3 and SnO_2 [30] were added to siloxane to produce superhydrophobic films to protect outdoor cultural heritage assets. Chatzigrigoriou [32] used dispersions of $Ca(OH)_2$ nanoparticles in siloxane emulsions to produce superhydrophobic coatings for marble protection, and the color change was 3.76, which was accepted for conservation purposes. In particular, ZnO nanoparticles [33] and Ag nanoparticles [34] were added to silicon-based consolidant/water-repellent materials, exerting biocide activity. It is worth mentioning that Karapanagiotis had done plenty of research about superhydrophobic materials for the conservation of natural stone and recently presented a detailed review [35]. These works have significantly developed the application of nanocomposite coatings in the field of stone heritage conservation.

However, less research has been done on the durability of nanocomposite coatings, and to the best of our knowledge, cases of the use of multiple-nanoparticle-modified organic coatings for cultural heritage protection are uncommon. As such, in this study, we modified DTMS with nano-SiO_2 and TiO_2 to fabricate superhydrophobic materials for application in sandstone protection. Their hydrophobicity, applicability, and durability for protecting sandstone-based cultural heritage were comprehensively studied. We investigated the effects of adding two kinds of nanoparticles, SiO_2 and TiO_2, separately and simultaneously, to thoroughly understand the role of nano-SiO_2 and TiO_2. Our findings contribute to the understanding of nanocomposite organic coatings and broaden the application of nanocomposites in the field of cultural heritage protection, providing more diverse materials for the protection of outdoor stone heritage.

2. Experimental

2.1. Preparation of Stone Samples

Red sandstone was acquired from the Daming Place Building Material Market, Xi'an. It was mainly composed of quartz, calcite, and feldspars, which were confirmed by XRD (see Supplementary Materials Figure S1 for details). The sandstone surface was cleaned with distilled water and then dried at 110 °C prior to the experiments. The specifications of the samples varied from test to test. Figure 1 shows the sample blocks used for different tests.

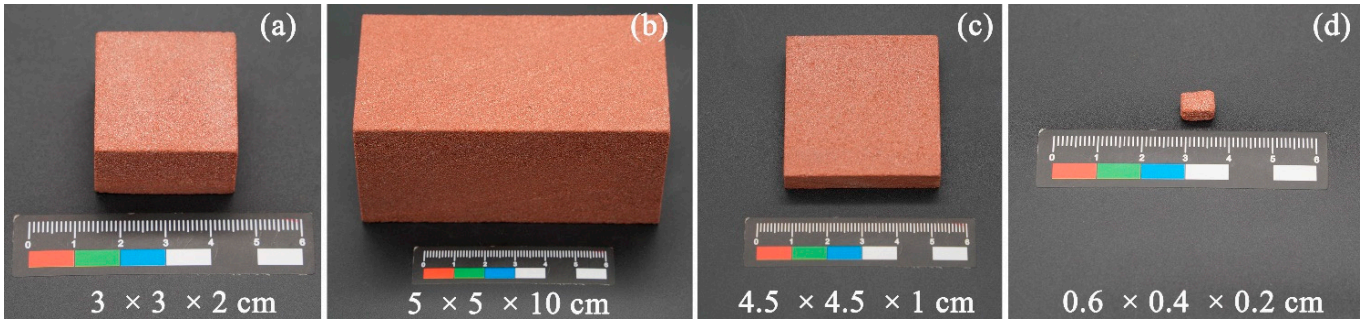

Figure 1. Stone samples used for the tests: (**a**) contact angle, color, thermal ageing, UVA ageing, chemical stability; (**b**) water absorption by capillarity; (**c**) water vapor permeability; (**d**) SEM.

2.2. Preparation and Application of Coatings

Dodecyltrimethoxysilane (DTMS, Sinopharm, Beijing, China), OP-10 (Emulsifier, Aladdin, Shanghai, China), and iso-propanol (Tianjin Fuyu, China) were used as received. The silicon dioxide nanoparticles (fumed powder, Aladdin, Shanghai, China) had an average particle size of 7~40 nm and a specific surface area of 150 m^2/g. The titanium dioxide nanoparticles (P25, Macklin, Shanghai, China) had an average particle size of 20 nm. The P25 TiO_2 consisted of two crystalline forms, anatase and rutile, in a 4:1 ratio. The nanoparticles were dried at 110 °C for 12 h before use.

Table 1 shows the formulations of the four prepared materials. The solutions were dispersed by using a high-speed shear dispersion tester for 5 min (6000 rpm) and then ultrasonicated for 30 min (36 kHz, 12 °C). The nanocomposites show excellent properties only if the nanoparticles are well-dispersed [36].

Table 1. Coating formulations in percent (*w/w*). D, dodecyltrimethoxysilane (DTMS); DT and DS, TiO_2- and SiO_2-modified DTMS, respectively; DST, TiO_2 and SiO_2 comodified DTMS, where iso-propanol was the solvent, OP-10 was the emulsifier, and the concentrations of TiO_2 and SiO_2 were 0.01% (*w/w*) and 0.5% (*w/w*), respectively.

Product	DTMS	Nano-TiO_2	Nano-SiO_2	Iso-Propanol	OP-10
D	10	-	-	90	-
DT	10	0.01	-	90	0.2
DS	10	-	0.5	90	0.2
DST	10	0.01	0.5	90	0.2

The solutions were applied dropwise to the stone surfaces using a Dlab graduated pipette (accuracy ± 1 μL, Beijing, China). One side of the sample was treated twice with the nanocomposite dispersion solutions, with 40 $\mu L/cm^2$ each time, in an interval of 1 h and a cumulative dosage of 80 $\mu L/cm^2$. The treated stones were subjected to 80 °C for two days and then to room temperature for more than two days.

2.3. Characterisation Tests

2.3.1. Morphological Observation

The sample surface micromorphology was determined using a field-emission scanning electron microscope (FESEM; Thermo scientific, Apros S, Waltham, MA, USA) with a 10 kV high voltage and an 11 mm work distance.

2.3.2. Waterproofing Test

Water Contact Angle Test

A static contact angle measuring instrument (Chenghui, JGW-360, Chengde, China) was used for the test. To ensure repeatability, the sample was measured 10 s after placing a 5 µL drop of water on the treated sample surface. Each sample was measured seven times, and we reported the average value. The roll-off angle was measured with a roll-off angle platform.

Water Absorption Capillarity Test

Flat cotton (total thickness of approximately 7 mm) was placed in a clean plate, and distilled water was added until the cotton was completely soaked, ensuring the water level did not exceed the upper surface of the cotton and remained constant during the test [37]. Each sample was weighed and was placed on top of the cotton to absorb water until the weight was constant. The amount of water absorbed per unit area Q_i (kg·m^{-2}) at time t_i (s) was calculated as follows:

$$Q_i = \frac{m_i - m_0}{A} \quad (1)$$

where m_0 is the mass of the specimen at time t_0, in kilograms; m_i is the mass of the specimen at time t_i, in kilograms; A is the area of the specimen in contact with the bedding layer (cotton), in meters squared.

After 72 h of treatment, the weight was basically constant. The water absorption inhibition efficiency (WIE) was calculated as follows [38]:

$$\text{WIE } \% = \frac{m_{un} - m_t}{m_{un}} \times 100 \quad (2)$$

where m_{un} and m_t are the amounts of water absorbed after 72 h of treatment by the untreated sample (the red sandstone) and by the sample treated with waterproofing coatings, respectively.

2.3.3. Suitability Analysis

Colorimetric Measurements

The appearance of the sample was characterized using a colorimeter (X-rite, VS 450, MI, USA). We adopted the CIE $L^*a^*b^*$ color system, where L^* indicates luminosity, 0 indicates black, and 100 indicates white; a^*, which ranges from positive to negative, indicates colors from red to green; b^*, which ranges from positive to negative indicates colors from yellow to blue. The color difference ΔE was calculated as follows:

$$\Delta E = \sqrt{(\Delta L^*)^2 + (\Delta a^*)^2 + (\Delta b^*)^2} \quad (3)$$

where ΔL^*, Δa^*, and Δb^* are the variations in the L^*, a^*, and b^* values of the samples before and after treatment, respectively. Each sample was measured four times, and we reported the average.

Water Vapor Permeability Test

The stones that were both untreated and treated with coatings were subjected to a water vapor permeability test, following UNI EN 15803 [39]. Each cup was filled with equal amounts of K_2SO_4-saturated solution to regulate humidity at 97%. The devices were sealed with paraffin wax and were then placed in a constant-temperature and -humidity

chamber at 25 °C and 50% humidity. The devices were weighed every 48 h. The variation in weight, Δm, was calculated as the difference between the weight of the apparatus (in kg) at times t_0 and t_i. The water vapor flow rate through the specimen in the unit of time, G kg·s^{-1}), was calculated as the slope of the Δm vs. t curve. The water vapor permeability, δp (kg·m^{-1}·s^{-1}·Pa^{-1}), was calculated as follows:

$$\delta p = \frac{G}{A \times \Delta_{P_v}} \times D \quad (4)$$

where A is the test surface area, in square meters; Δ_{P_v} is the water vapor pressure difference across the samples, in Pascals; D is the thickness of the samples, in meters.

2.3.4. Durability Analysis

Stone relics, especially outdoors, are inevitably weathered by heat, ultraviolet rays, and some acidic and alkaline chemicals. Therefore, we tested the durability of the coating from three aspects:

Thermal Stability Test

The samples were placed in an oven at 180 °C to accelerate thermal ageing. The contact angles were periodically measured until the contact angle was below 60°, for a total ageing time of 252 h.

To study the difference in the thermal stability between DTMS before and after modifications, 5 mL of the nanocomposite solution was mixed with 1 g of sandstone powder. The mixture (6~7 mg) after completely curing was obtained for thermogravimetric analysis using a simultaneous thermal analyzer (Mettler Toledo, TGA-DSC3+, Zurich, Switzerland) in a nitrogen atmosphere with a flow rate of 20 mL·min^{-1} and a heating rate of 10 °C·min^{-1}.

UV Shielding Test

Of the UV radiation produced by the sun and received by the Earth, almost all the short-wave UVC (200–280 nm) is absorbed by the ozone layer, and about 2%–5% of the medium-wave UVB (280–320 nm) reaches the Earth. The rest of the UV radiation is long-wave UVA (320–400 nm). To simulate the UV radiation damage of outdoor stone artefacts, UVA was chosen as the light source for testing.

The samples were placed in a UV ageing chamber for ageing, where 5 identical UVA lamps (Philips, 8 W 365 nm) were installed. The sample surface was 16 cm from the base of the lamps with a UV irradiance (365 nm) of 10.35 W/m^2. The contact angles were measured every 24 h until the contact angle was below 60°, for a total ageing time of 144 h. The sample position was periodically changed during the experiment to ensure uniform ageing.

The ability of the added nanoparticles to shield against UV light was studied by using a UV–Visible spectrophotometer (Hitachi, U-2001, Tokyo, Japan) with a scanning speed of 200 nm/min. Approximately 4 mL of the solution prepared as described in Section 2.2 was tested. Iso-propanol as the reference solution and a 1 cm thick quartz cuvette were used.

Chemical Durability Test

The samples were immersed in pH 1, 7 (ultrapure water), or 13 solutions for 24 h. The contact angles of the samples before and after treatment were measured.

3. Results and Discussion

3.1. Water-Repellence Performance

3.1.1. Contact Angle

The static contact angles of the samples are reported in Table 2, where S represents untreated sandstone. These images are shown in Figure 2. DTMS (Figure 2a) showed suitable water resistance with a contact angle of 126.5°, and the addition of 0.01% TiO_2 to DTMS (Figure 2b) produced an insignificant improvement in the contact angle of DTMS. Adding 0.5% SiO_2 to DTMS (Figure 2c,d) resulted in a substantial increase in the contact angle

beyond 150°, with a roll-off angle of less than 10° measured using a roll-off angle platform. Because the static contact angle was larger than 150° and the roll-off angle was less than 10°, the fabricated nanocomposite DS and DST coatings were superhydrophobic materials.

Table 2. Average values of the static contact angles (θ) and water vapor permeability (δp).

Sample	θ (°)	δp (10^{-11} kg·(m·s·Pa)$^{-1}$)	RP (%)
S	0	1.34 ± 0.06	100.00
D	126.5 ± 6.4	1.13 ± 0.04	84.17
DT	129.3 ± 3.4	1.10 ± 0.05	82.15
DS	152.5 ± 3.5	1.12 ± 0.07	83.68
DST	152.1 ± 2.6	1.14 ± 0.04	84.83

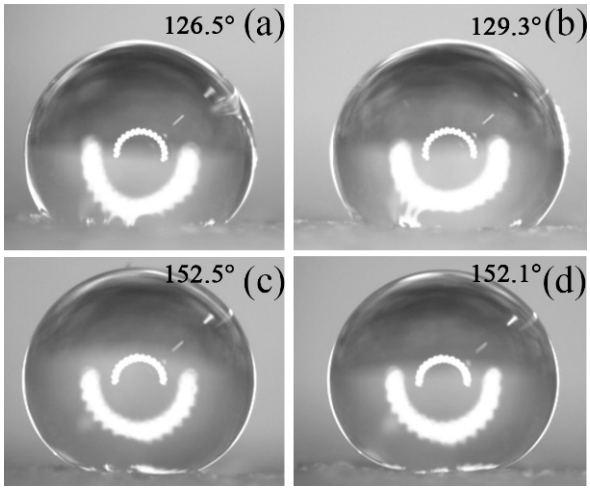

Figure 2. Static contact angle images: (**a**) D; (**b**) DT; (**c**) DS; (**d**) DST.

3.1.2. Water Absorption by Capillarity

The amount of water absorbed by the samples per unit of area Q_i over time is reported in Figure 3. Compared with the untreated samples, the samples treated with DTMS and nanocomposite coatings all had a WIE higher than 92% after 72 h of absorption, showing excellent water-repellence performance.

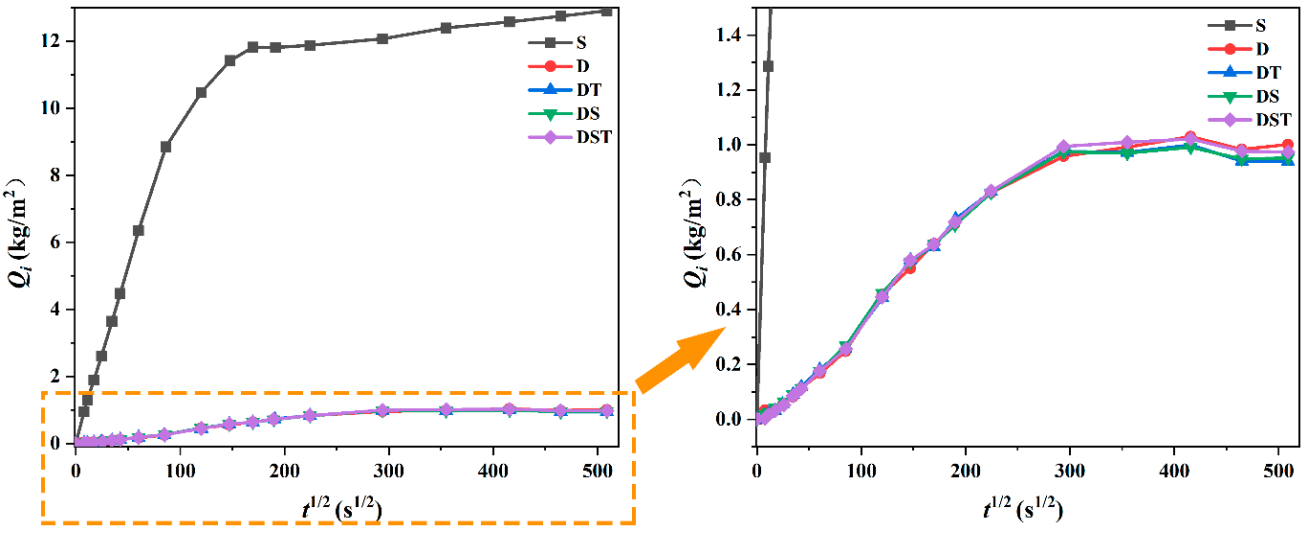

Figure 3. Capillary water-absorption curves.

3.2. Micromorphology

The SEM images of the samples (Figure 4) showed that the original sandstone surface (Figure 4a) was relatively rough. After coating with DTMS, a relatively smooth and low-surface-energy surface formed (Figure 4b), and the latter mainly imparted hydrophobicity to the surface. After the addition of TiO_2 nanoparticles to DTMS, a low content (0.01% *w/w*) of TiO_2 nanoparticles was sporadically distributed on the stone surface (Figure 4c), which was unable to produced sufficient roughness, thereby minimally affecting the contact angle of DTMS. The SiO_2 nanoparticles (0.5% *w/w*) were able to more uniformly gather on the stone surface, forming a rough structure (Figure 4d,e). When water drops fell on the DS and DST surfaces, the air was trapped in the void between the water and rough structure formed by the accumulation of nanoparticles, and the drops thus easily rolled off, which is in accordance with the Cassie–Baxter model [13,14].

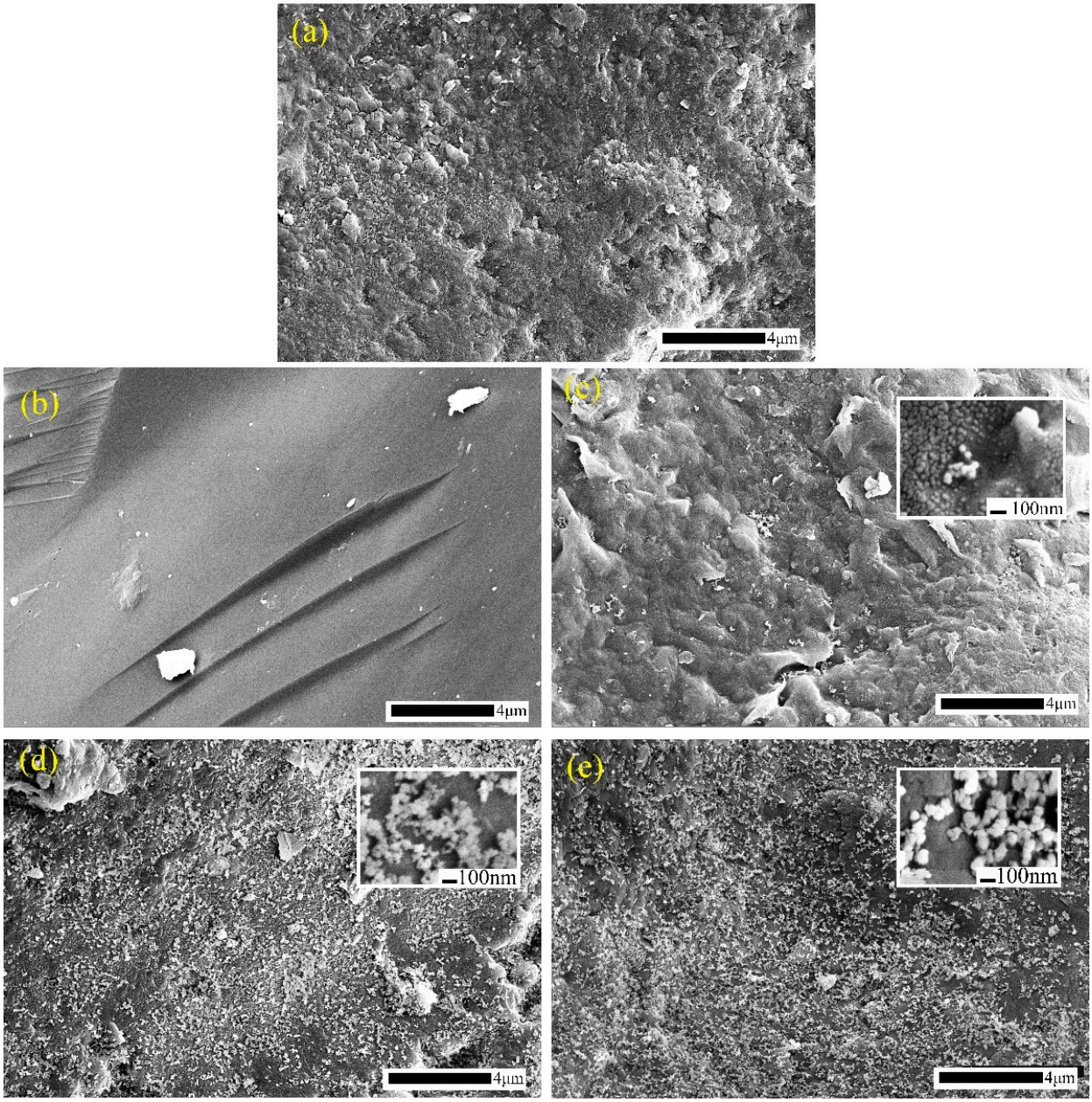

Figure 4. SEM images: (**a**) S, (**b**) D, (**c**) DT, (**d**) DS, and (**e**) DST. A higher-magnification image is depicted in (**c**,**d**), and (**e**) in the upper right corner.

It has been reported that different types of nanoparticles can form rough structures to achieve superhydrophobicity [30]. For elevated particle concentration, the wettabilities of the surfaces were not affected by the original particle sizes of the nanomaterials [40,41]. Nevertheless, adequate roughness of the substrate surface at the high nanoparticle concentration is a key condition for achieving superhydrophobicity [40]. Therefore, adding low concentrations of TiO_2 nanoparticles had little effect on the contact angle of DTMS, while high concentrations of SiO_2 nanoparticles greatly increased the contact angle.

According to the SEM image in Figure 4e, the DST particle size (Figure 5) was calculated as almost 70% in the range of 60~90 nm, with an average particle size of 81 nm, indicating that the nanoparticles were well-dispersed and formed a rough nanoscale structure.

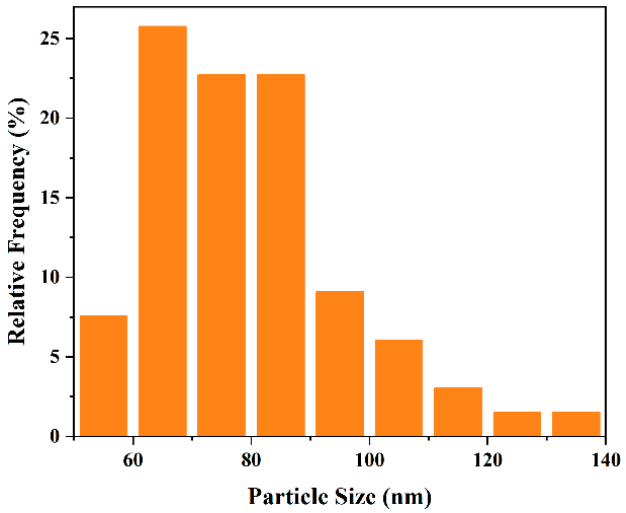

Figure 5. Particle size distribution of DST.

3.3. Suitability

3.3.1. Color Change

The color variation in the samples before and after treatment is shown in Figure 6. The color changes in the samples were mainly produced by ΔL^*, which was due to the application of the protective materials causing the stone surface to slightly darken, resulting in a slight decrease in L^*. However, the decrease in L^* was less than two. Both Δa^* and Δb^* were less than 0.5, indicating a small change in the coatings' red–green and yellow–blue coordinates and good transparency. Because of the good dispersion, no severe agglomeration of nanoparticles occurred to cover the original appearance of the stone surface, which maintained the excellent optical transparency of DTMS. There was no notable difference between adding only one nanoparticle or two nanoparticles at the same time, both of which had an ΔE of less than two, which did not change the color of the stones and met the requirement of $\Delta E < 5$ for materials used for stone conservation [42,43].

3.3.2. Water Vapor Permeability

Generally, the water vapor permeability of stone should remain unchanged after being treated with the ideal protective material; that is, the coating hinders the transport of liquid water but not that of water vapor. Water condensation underneath the protective layer leads to crispy alkali damage to the stone as a result of expansion and contraction under dry–wet cycles and contributes to the loss of adhesion and of the protective effects of the coating [31,44].

The water vapor permeability, δp, is shown in Table 2, and RP, the relative water vapor permeability, is the ratio of the water vapor permeability of the coated sample to the uncoated sandstone. The stone treated with DTMS and nanocomposite coatings maintained a relative water vapor permeability higher than 82% compared with the original sandstone, which meant they all had excellent water vapor permeability.

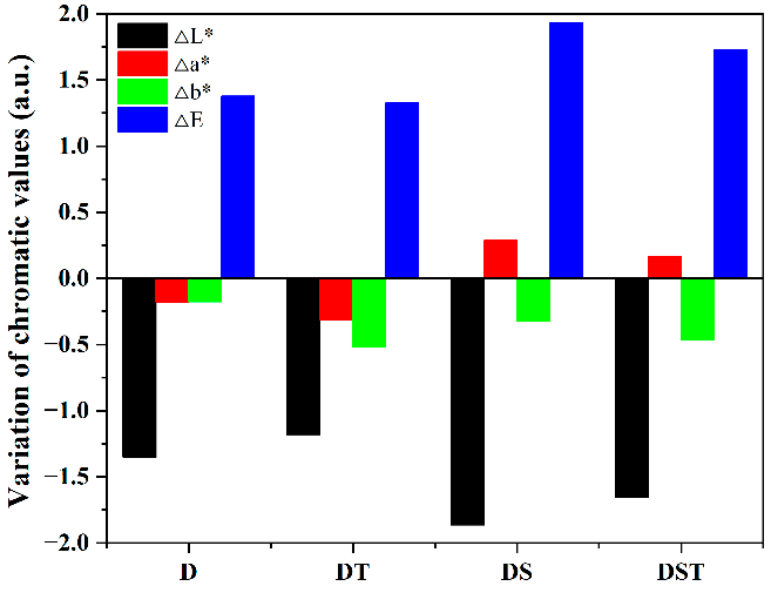

Figure 6. Variation in chromatic values before and after treatment.

3.4. Durability

3.4.1. Thermal Stability

Figure 7 shows the variation of the static contact angles (SCAs) of the samples during the thermal ageing test. Adding both TiO_2 and SiO_2 improved the heat resistance of DTMS, and DST was the most thermally stable.

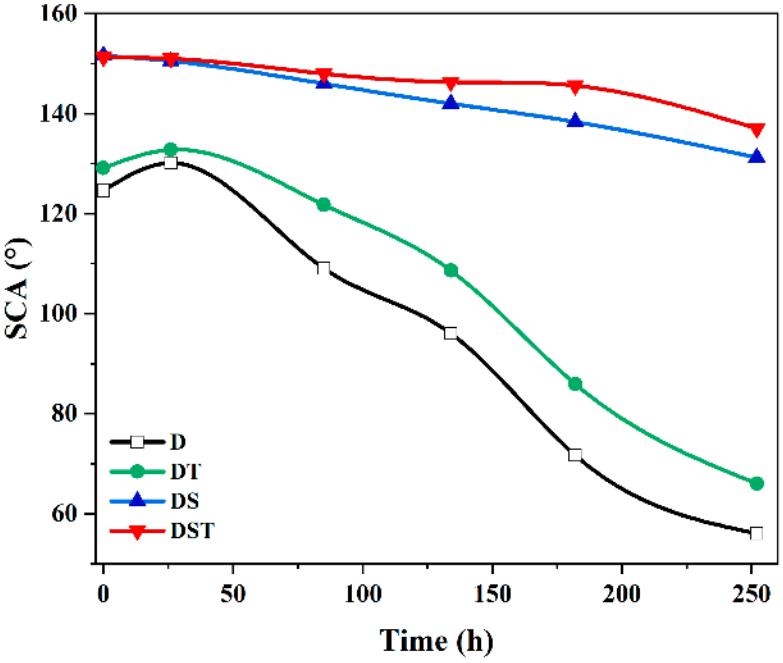

Figure 7. Variation in the static contact angles during the thermal ageing test.

Figure 8 shows the TG and DTG curves (the micro-quotient thermogravimetric curves) of the samples. As the coated sandstones were used as samples, the vast majority of which are mineral, there was minimal weight loss. The interval from 300 to 600 °C was chosen for our study because of minimal weight loss below 400 °C.

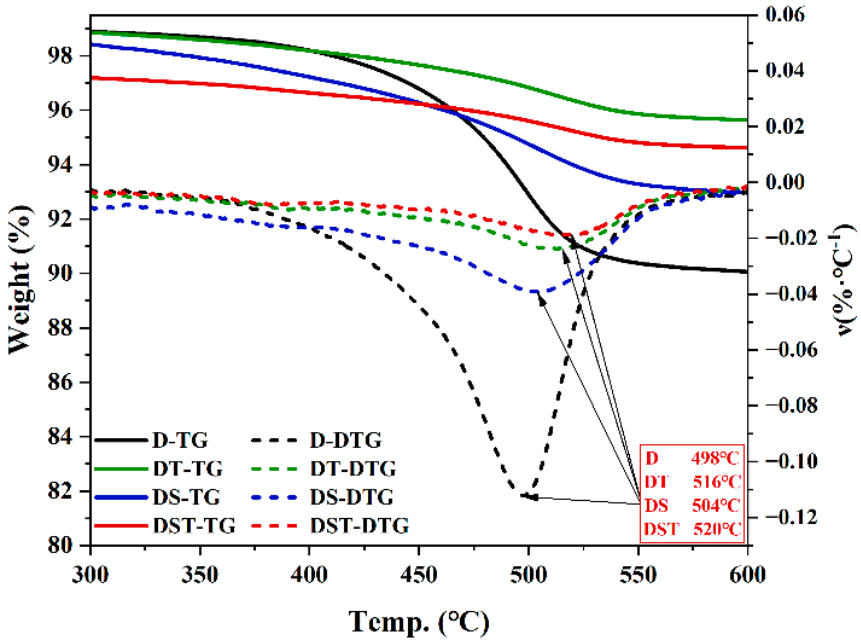

Figure 8. TG curves (solid lines) and DTG curves (dotted lines). Arrows point to maximum rates of weight loss. Values of temperature at the maximum rates of weight loss are provided in the lower right corner.

From the DTG curves in Figure 8, we found that the maximum weight loss rates occurred at 498 °C for DTMS, 516 °C for DT, 504 °C for DS, and 520 °C for DST. The rise in the maximum decomposition peak temperature values indicates an increase in thermal stability [45]. Therefore, the thermal stability of three modified coatings was improved compared with that of DTMS, where that of DT was improved more than that of DS. The two types of nanoparticles had a synergistic effect, so DST showed the highest thermal stability.

TiO_2 [46] and SiO_2 are both inorganic fire-retardant materials that can form passivation layers on a coating surface during thermal degradation. They can also act as insulators and/or mass transfer barriers to the volatile byproducts generated during thermal decomposition [47,48]. Additionally, increased thermal stability is related to the strong hydrogen bonding interactions of the nanoparticle and substrate, which impede the mobility of the molecular chains [49] and inhibit the attacks of free radicals on the main chain [45].

3.4.2. UV Shielding Performance

According to Rayleigh's theory, when the particle size is much smaller than the wavelength of the incident light, the intensity of the scattered light is inversely proportional to the fourth power of the incident wavelength ($I \propto \frac{1}{\lambda^4}$). Nanoparticles have strong UV light absorption and scattering effects because of their small particle size. With suitable dispersion, the addition of nanoparticles to coatings may provide shield from UV light [45,50] and improve the durability of coatings.

The variation in the contact angles of the samples during the UVA ageing test is shown in Figure 9. Compared with D, the UVA resistance of DT was lower. This may have been due to the photocatalytic activity of TiO_2 under UV light, which degraded DTMS under UVA irradiation [51], causing a decrease in its original hydrophobic property. Another explanation is that TiO_2 is photophilic [52] and hydrophilic under UV radiation, adsorbing invisible water films and causing a decrease in the contact angle [53].

The UVA resistance of DS was substantially stronger than that of D. After 144 h of UVA irradiation, the contact angle of D was 84.0°, whereas that of DS was 124.3°. The UVA resistance of DST was consistent with that of DS with no additional decrease, presumably

due to the low concentration of TiO_2, which produced a negative effect that could be neglected compared with the UV shielding effect of SiO_2.

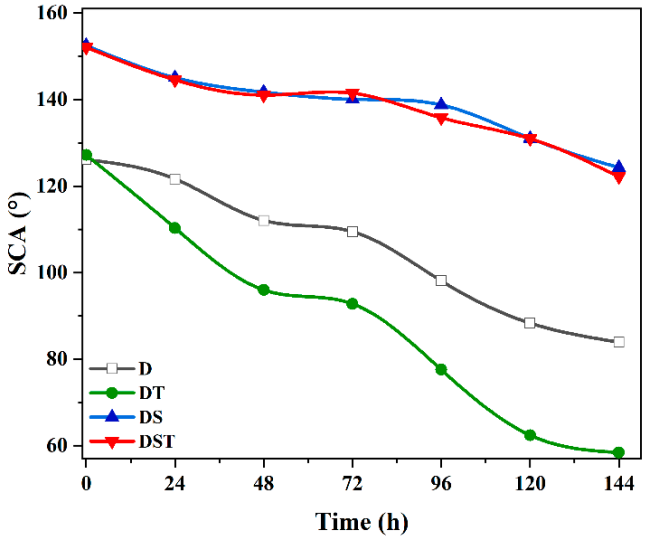

Figure 9. Variation in static contact angles during the UVA ageing test.

Figure 10 shows the transmittance–wavelength curves (solid lines) for different solutions in various UV regions: for the UVA, UVB, and UVC (200–400 nm) region and for the UVA (320–400 nm) region, the most common band in sunlight. The curves were integrated, which are shown as dashed lines in Figure 10. The UV resistance of the materials can be expressed by the shielding efficiency, which is calculated as follows [54]:

$$\eta_1 = \left(1 - \frac{\int_{200}^{400} T_{NP}(\lambda)d\lambda}{\int_{200}^{400} T_D(\lambda)d\lambda}\right) \times 100\% \quad (5)$$

$$\eta_2 = \left(1 - \frac{\int_{320}^{400} T_{NP}(\lambda)d\lambda}{\int_{320}^{400} T_D(\lambda)d\lambda}\right) \times 100\% \quad (6)$$

where η_1 and η_2 are the efficiency in shielding from 200–400 and 320–400 nm ultraviolet rays, respectively; $T(\lambda)$ is the average value of the spectral transmittance of the material; $d\lambda$ is the bandwidth; and λ is the wavelength. T_D is for the DTMS curve, and T_{NP} is DT, DS, or DST.

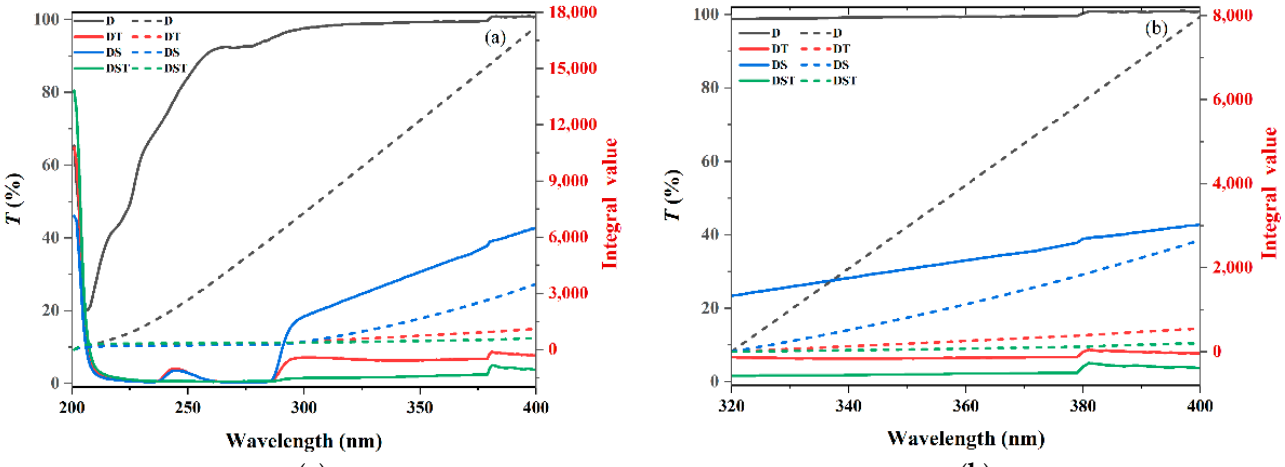

Figure 10. UV–Vis spectra of different groups of solutions in solid lines and integral values of the curves (right Y-axis) represented by dotted lines: (**a**) 200–400 nm; (**b**) 320–400 nm.

The shielding efficiency calculation is reported in Table 3. We found a strong UV shielding when SiO_2 and TiO_2 nanoparticles were added to DTMS. SiO_2 (0.5%) shielded nearly 80% of the UV in the 200–400 nm band and more than two-thirds of the most common UVA in sunlight. Low doses (0.01%) of TiO_2 shielded more than 93% of the whole wavelength band and the most common UVA bands. The mixture of the two nanoparticles synergistically shielded more than 95% and 97% of UV (200–400 nm) and UVA, respectively.

Table 3. UV shielding efficiency of the nanocomposite coatings.

Sample	$\int_{200}^{400} T(\lambda)d\lambda$	$\int_{320}^{400} T(\lambda)d\lambda$	η_1	η_2
D	17,292.80	7969.70	0	0
DT	1166.85	550.60	93.25	93.09
DS	3524.35	2636.80	79.62	66.91
DST	696.00	204.35	95.98	97.44

Combined with the result of UVA ageing, we found that TiO_2 had a high UV shielding efficiency but reduced the contact angle of coatings because the ultraviolet light shielded by TiO_2 does not safely radiate, which has a harmful effect on the coating [55,56]. Adding SiO_2 led to a safe radiation of the shielded ultraviolet, which prevented this adverse effect. DST still showed suitable UV shielding performance.

3.4.3. Chemical Stability

Figure 11 shows the changes in the contact angles of the samples immersed in solutions with different pH values for 24 h. The results showed that (1) The contact angle value of D and nanocomposites decreased the most (about 30°) under acidic conditions, and the heterogeneity increased (higher values of standard deviation), mainly because the sandstone contains calcite, which is dissolved under strongly acidic conditions, so the sandstone was structurally damaged, and many crystals precipitated on the surfaces (see the micromorphology of the samples in the Supplementary Materials Figure S2). The contact angle values of D, DT, and DS generally decreased by less than 5° after neutral water immersion, whereas that of DST remained unchanged. Under alkaline conditions, it only decreased by about 10°. (2) Adding nanoparticles to coatings, especially SiO_2, ensures the coating retains suitable hydrophobicity after immersion and improves its chemical stability.

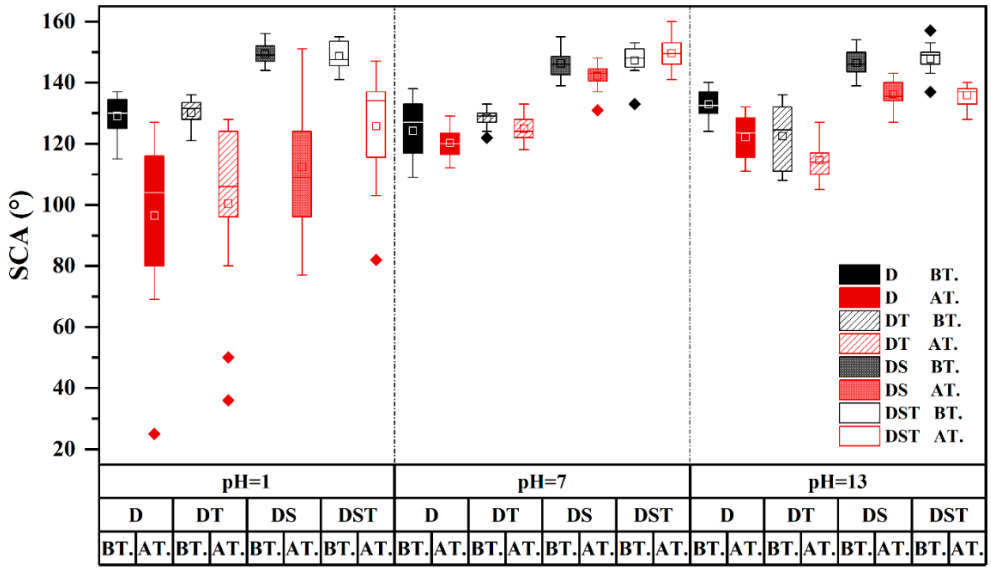

Figure 11. Changes in the contact angles of the samples immersed in solutions with different pH values for 24 h. BT, before treatment; AT, after treatment.

4. Conclusions

In this study, TiO_2 and SiO_2 nanoparticles were used to modify DTMS, a commonly used waterproof coating for stone artefacts, to fabricate nanocomposite coatings. We characterized the micromorphology, water-repellence, suitability for protecting stone heritage, and durability of the coatings. The results showed that the nanoparticles were well-dispersed in the coating, with 70% of the particle size of DST distributed in the range of 60 to 90 nm, with an average particle size of 81 nm, forming a rough nanoscale structure. The nanocomposite coatings had a minimal effect on the appearance of the stone, $\Delta E < 2$, and more than 82% of the water vapor permeability of the uncoated sandstone was retained, demonstrating suitability for stone artefact protection. The nanoparticles were added to DTMS: TiO_2 (0.01% *w/w*) failed to produce sufficient roughness and so had no impact on the contact angle of the coating but improved the thermal stability; SiO_2 (0.5% *w/w*) produced sufficient roughness, which made the coating superhydrophobic with a contact angle of more than 152° and improved the thermal, light, and chemical durability. When nano-TiO_2 and SiO_2 were simultaneously added, the nano-SiO_2 mitigated the effects of nano-TiO_2 accelerating UVA ageing and improved the original thermal stability, UVA shielding ability, and chemical stability of DTMS, resulting in a significant improvement in durability and DST showed the best overall performance.

The nano-SiO_2-TiO_2/DTMS, a superhydrophobic coating, fabricated in this study, has excellent properties, a low cost, and is simple to prepare and apply, showing promise as a material for protecting outdoor stone heritage.

Supplementary Materials: The following supporting information can be downloaded at https://www.mdpi.com/article/10.3390/coatings12101397/s1, Figure S1: XRD pattern of sandstone used in this study; Figure S2: Micromorphological images of the samples tested for chemical stability.

Author Contributions: M.P.: Investigation, Writing–original draft, Writing—review & editing. L.W.: Investigation, Supervision, Writing—review. L.G.: Investigation, Writing—review. J.G.: Investigation. L.Z.: Investigation. F.Y.: Investigation. Z.M.: Writing—review & editing. X.Z.: Supervision, Writing—review & editing. All authors have read and agreed to the published version of the manuscript.

Funding: This research was supported by the National Natural Science Foundation of China (52203126), the Key Research and Development Plan of Shaanxi Province (2019ZDLSF07-05, 2022SF-321), Projects of the Social Science Foundation of Shaanxi Province (2021G001), the Education Department of Shaanxi Province (20JZ092), National Social Science Fund of China (17XKG002), and School of Cultural Heritage, Northwest University (2020WYYCY-02), 111 Project (D18004).

Institutional Review Board Statement: Not applicable.

Informed Consent Statement: Not applicable.

Data Availability Statement: The datasets used and/or analyzed during the current study are available from the corresponding author on reasonable request.

Acknowledgments: We thank the Laboratory Technicians, Hongna Xing and Shuai Chang, of the Communion Center of Analysis & Measurement, School of Physics, Northwest University for the SEM and XRD analysis, respectively. Thanks to Yunlu Ma for her enlightening suggestions for data analysis.

Conflicts of Interest: The authors declare no conflict of interest.

References

1. Liu, R.; Zhang, B.; Zhang, H.; Shi, M. Deterioration of Yungang Grottoes: Diagnosis and research. *J. Cult. Herit.* **2011**, *12*, 494–499. [CrossRef]
2. Kaur, G.; Singh, S.; Kaur, P.; Garg, S.; Fareeduddin; Pandit, M.K.; Agrawal, P.; Acharya, K.; Ahuja, A. Vindhyan Sandstone: A Crowning Glory of Architectonic Heritage from India. *Geoheritage* **2019**, *11*, 1771–1783. [CrossRef]
3. Centauro, I.; Vitale, J.G.; Calandra, S.; Salvatici, T.; Natali, C.; Coppola, M.; Intrieri, E.; Garzonio, C.A. A Multidisciplinary Methodology for Technological Knowledge, Characterization and Diagnostics: Sandstone Facades in Florentine Architectural Heritage. *Appl. Sci.* **2022**, *12*, 4266. [CrossRef]

4. Rihosek, J.; Bruthans, J.; Masin, D.; Filippi, M.; Carling, G.T.; Schweigstillova, J. Gravity-induced stress as a factor reducing decay of sandstone monuments in Petra, Jordan. *J. Cult. Herit.* **2016**, *19*, 415–425. [CrossRef]
5. Migoń, P. Geoheritage and World Heritage Sites. *Geoheritage* **2018**, *13*, 237–249. [CrossRef]
6. Siegesmund, S.; Snethlage, R. *Stone in Architecture*; Springer: Berlin/ Heidelberg, Germany, 2011; p. 227. ISBN 978-3-642-14474-5.
7. Cao, Y.; Salvini, A.; Camaiti, M. One-step fabrication of robust and durable superamphiphobic, self-cleaning surface for outdoor and in situ application on building substrates. *J. Colloid Interface Sci.* **2021**, *591*, 239–252. [CrossRef]
8. Colangiuli, D.; Lettieri, M.; Masieri, M.; Calia, A. Field study in an urban environment of simultaneous self-cleaning and hydrophobic nanosized TiO_2-based coatings on stone for the protection of building surface. *Sci. Total Environ.* **2019**, *650*, 2919–2930. [CrossRef]
9. Pargoletti, E.; Motta, L.; Comite, V.; Fermo, P.; Cappelletti, G. The hydrophobicity modulation of glass and marble materials by different Si-based coatings. *Prog. Org. Coat.* **2019**, *136*, 105260. [CrossRef]
10. Serra, C.L.; Tulliani, J.-M.; Sangermano, M. An Acrylic Latex Filled with Zinc Oxide by Miniemulsion Polymerization as a Protective Coating for Stones. *Macromol. Mater. Eng.* **2014**, *299*, 1352–1361. [CrossRef]
11. Ruffolo, S.A.; La Russa, M.F. Nanostructured Coatings for Stone Protection: An Overview. *Front. Mater.* **2019**, *6*, 147. [CrossRef]
12. Cassie, A.B.D.; Baxter, S. Wettability of porous surfaces. *Trans. Faraday Soc.* **1944**, *40*, 546. [CrossRef]
13. Xue, C.; Jia, S.; Zhang, J.; Ma, J. Large-area fabrication of superhydrophobic surfaces for practical applications: An overview. *Sci. Technol. Adv. Mater.* **2010**, *11*, 33002. [CrossRef] [PubMed]
14. Saji, V.S. Electrophoretic-deposited Superhydrophobic Coatings. *Chem. Asian J.* **2021**, *16*, 474–491. [CrossRef]
15. Li, M.; Yang, Y.-Q.; Liu, L.; Hu, J.; Zhang, J. Electro-assisted preparation of dodecyltrimethoxysilane/TiO_2 composite films for corrosion protection of AA2024-T3 (aluminum alloy). *Electrochim. Acta* **2010**, *55*, 3008–3014. [CrossRef]
16. Zhang, S.; Cao, D.; Xu, L.; Tang, J.; Meng, R.; Li, H. Corrosion resistance of a superhydrophobic dodecyltrimethoxysilane coating on magnesium hydroxide-pretreated magnesium alloy AZ31 by electrodeposition. *Colloids Surf. A* **2021**, *625*, 126914. [CrossRef]
17. Xu, B.; Cai, Z. Fabrication of a superhydrophobic ZnO nanorod array film on cotton fabrics via a wet chemical route and hydrophobic modification. *Appl. Surf. Sci.* **2008**, *254*, 5899–5904. [CrossRef]
18. Zheng, L.; Chen, Y. Research on the Restoration Techniques and Prevention Strategies of Historic Buildings in Macao. *IOP Conf. Ser. Earth Environ. Sci.* **2021**, *783*, 12111. [CrossRef]
19. Zheng, L.; Chen, Y. Problems and countermeasures in the restoration project of cultural relics of Macao Chong Sai Pharmacy. *E3S Web Conf.* **2021**, *284*, 5005. [CrossRef]
20. Ling, H.; Maiqian, N.; Guozheng, L. Preparation and feasibility analysis of fluoropolymer to the sandstone protection. *Prog. Org. Coat.* **2008**, *62*, 206–213. [CrossRef]
21. Zhen, G. Application of WD-10 in the surface protection of the lithoid cultural relic. *New Chem. Mater.* **2001**, 48–50. Available online: https://www.cnki.com.cn/Article/CJFDTOTAL-HGXC200109011.htm (accessed on 29 August 2022).
22. Wang, H.; Feng, N.; Song, D. Study of conservation method for the weathering of Goguryeo stone heritage. *Relics Museol.* **2010**, 76–81. Available online: https://www.cnki.com.cn/Article/CJFDTOTAL-WEBO201006017.htm (accessed on 29 August 2022).
23. Wang, L.; Li, Y.; Zhao, X. Modification of WD-10, a waterproof material for stone relics, with nano TiO_2. *Fine Chem.* **2015**, *32*, 250–253. Available online: https://www.cnki.com.cn/Article/CJFDTOTAL-JXHG201503003.htm (accessed on 29 August 2022). [CrossRef]
24. Baglioni, P.; Carretti, E.; Chelazzi, D. Nanomaterials in art conservation. *Nat. Nanotechnol.* **2015**, *10*, 287–290. [CrossRef] [PubMed]
25. Franco-Castillo, I.; Hierro, L.; de La Fuente, J.M.; Seral-Ascaso, A.; Mitchell, S.G. Perspectives for antimicrobial nanomaterials in cultural heritage conservation. *Chem* **2021**, *7*, 629–669. [CrossRef]
26. Honarvar Nazari, M.; Zhang, Y.; Mahmoodi, A.; Xu, G.; Yu, J.; Wu, J.; Shi, X. Nanocomposite organic coatings for corrosion protection of metals: A review of recent advances. *Prog. Org. Coat.* **2022**, *162*, 106573. [CrossRef]
27. Dalawai, S.P.; Saad Aly, M.A.; Latthe, S.S.; Xing, R.; Sutar, R.S.; Nagappan, S.; Ha, C.; Kumar Sadasivuni, K.; Liu, S. Recent Advances in durability of superhydrophobic self-cleaning technology: A critical review. *Prog. Org. Coat.* **2020**, *138*, 105381. [CrossRef]
28. Frigione, M.; Lettieri, M. Novel attribute of organic–inorganic hybrid coatings for protection and preservation of materials (stone and wood) belonging to cultural heritage. *Coatings* **2018**, *8*, 319. [CrossRef]
29. Facio, D.S.; Mosquera, M.J. Simple strategy for producing superhydrophobic nanocomposite coatings in situ on a building substrate. *ACS Appl. Mater. Interfaces* **2013**, *5*, 7517–7526. [CrossRef]
30. Manoudis, P.N.; Karapanagiotis, I.; Tsakalof, A.; Zuburtikudis, I.; Kolinkeová, B.; Panayiotou, C. Superhydrophobic films for the protection of outdoor cultural heritage assets. *Appl. Phys. A* **2009**, *97*, 351–360. [CrossRef]
31. Caponetti, E.; Ciaramitaro, V.; Armetta, F.; Renda, V.; Ercoli, L.; Saladino, M.L. Effectiveness of some protective and self-cleaning treatments: A challenge for the conservation of temple G stone in Selinunte. *Prog. Org. Coat.* **2021**, *151*, 106020. [CrossRef]
32. Chatzigrigoriou, A.; Karapanagiotis, I.; Poulios, I. Superhydrophobic coatings based on siloxane resin and calcium hydroxide nanoparticles for marble protection. *Coatings* **2020**, *10*, 334. [CrossRef]
33. Ditaranto, N.; Van der Werf, I.D.; Picca, R.A.; Sportelli, M.C.; Giannossa, L.C.; Bonerba, E.; Tantillo, G.; Sabbatini, L. Characterization and behaviour of ZnO-based nanocomposites designed for the control of biodeterioration of patrimonial stoneworks. *New J. Chem.* **2015**, *39*, 6836–6843. [CrossRef]

34. Essa, A.M.; Khallaf, M.K. Biological nanosilver particles for the protection of archaeological stones against microbial colonization. *Int. Biodeterior. Biodegrad.* **2014**, *94*, 31–37. [CrossRef]
35. Karapanagiotis, I.; Manoudis, P.N. Superhydrophobic and superamphiphobic materials for the conservation of natural stone: An overview. *Constr. Build. Mater.* **2022**, *320*, 126175. [CrossRef]
36. La Russa, M.F.; Rovella, N.; Alvarez de Buergo, M.; Belfiore, C.M.; Pezzino, A.; Crisci, G.M.; Ruffolo, S.A. Nano-TiO_2 coatings for cultural heritage protection: The role of the binder on hydrophobic and self-cleaning efficacy. *Prog. Org. Coat.* **2016**, *91*, 1–8. [CrossRef]
37. *UNI EN 15801:2010*; Conservation of Cultural Property-Test Methods—Determination of Water Absorption by Capillarity. UNI Ente Nazionale Italiano di Unificazione: Milan, Italy, 2010.
38. Camaiti, M.; Brizi, L.; Bortolotti, V.; Papacchini, A.; Salvini, A.; Fantazzini, P. An Environmental Friendly Fluorinated Oligoamide for Producing Nonwetting Coatings with High Performance on Porous Surfaces. *ACS Appl. Mater. Interfaces* **2017**, *9*, 37279–37288. [CrossRef] [PubMed]
39. *UNI EN 15803:2010*; Conservation of Cultural Property-Test Methods—Determination of Water Vapour Permeability. UNI Ente Nazionale Italiano di Unificazione: Milan, Italy, 2010.
40. Karapanagiotis, I.; Manoudis, P.N.; Savva, A.; Panayiotou, C. Superhydrophobic polymer-particle composite films produced using various particle sizes. *Surf. Interface Anal.* **2012**, *44*, 870–875. [CrossRef]
41. Manoudis, P.N.; Karapanagiotis, I. Modification of the wettability of polymer surfaces using nanoparticles. *Prog. Org. Coat.* **2014**, *77*, 331–338. [CrossRef]
42. La Russa, M.F.; Ruffolo, S.A.; Rovella, N.; Belfiore, C.M.; Palermo, A.M.; Guzzi, M.T.; Crisci, G.M. Multifunctional TiO_2 coatings for Cultural Heritage. *Prog. Org. Coat.* **2012**, *74*, 186–191. [CrossRef]
43. García, O.; Malaga, K. Definition of the procedure to determine the suitability and durability of an anti-graffiti product for application on cultural heritage porous materials. *J. Cult. Herit.* **2012**, *13*, 77–82. [CrossRef]
44. Lettieri, M.; Masieri, M.; Frigione, M. Durability to simulated bird guano of nano-filled oleo/hydrophobic coatings for the protection of stone materials. *Prog. Org. Coat.* **2020**, *148*, 105900. [CrossRef]
45. Loste, J.; Lopez-Cuesta, J.-M.; Billon, L.; Garay, H.; Save, M. Transparent polymer nanocomposites: An overview on their synthesis and advanced properties. *Prog. Polym. Sci.* **2019**, *89*, 133–158. [CrossRef]
46. Zhou, L.; Fu, Y. Flame-Retardant Wood Composites Based on Immobilizing with Chitosan/Sodium Phytate/Nano-TiO_2-ZnO Coatings via Layer-by-Layer Self-Assembly. *Coatings* **2020**, *10*, 296. [CrossRef]
47. Cai, Y.; Ke, H.; Dong, J.; Wei, Q.; Lin, J.; Zhao, Y.; Song, L.; Hu, Y.; Huang, F.; Gao, W.; et al. Effects of nano-SiO_2 on morphology, thermal energy storage, thermal stability, and combustion properties of electrospun lauric acid/PET ultrafine composite fibers as form-stable phase change materials. *Appl. Energy* **2011**, *88*, 2106–2112. [CrossRef]
48. Díez-Pascual, A.M.; Xu, C.; Luque, R. Development and characterization of novel poly(ether ether ketone)/ZnO bionanocomposites. *J. Mater. Chem. B* **2014**, *2*, 3065–3078. [CrossRef] [PubMed]
49. Díez-Pascual, A.M.; Díez-Vicente, A.L. Nano-TiO_2 reinforced PEEK/PEI blends as biomaterials for load-bearing implant applications. *ACS Appl. Mater. Interfaces* **2015**, *7*, 5561–5573. [CrossRef] [PubMed]
50. Liu, H; Hu, D.; Chen, X.; Ma, W. Surface engineering of nanoparticles for highly efficient UV -shielding composites. *Polym. Adv. Technol.* **2021**, *32*, 6–16. [CrossRef]
51. Li, W.; Lin, J.; Zhao, Y.; Pan, Z. The Adverse Effects of TiO_2 Photocatalycity on Paraloid B72 Hybrid Stone Relics Protective Coating Aging Behaviors under UV Irradiation. *Polymers* **2021**, *13*, 262. [CrossRef]
52. Wang, R.; Hashimoto, K.; Fujishima, A.; Chikuni, M.; Kojima, E.; Kitamura, A.; Shimohigoshi, M.; Watanabe, T. Light-induced amphiphilic surfaces. *Nature* **1997**, *388*, 431–432. [CrossRef]
53. Colangiuli, D.; Calia, A.; Bianco, N. Novel multifunctional coatings with photocatalytic and hydrophobic properties for the preservation of the stone building heritage. *Constr. Build. Mater.* **2015**, *93*, 189–196. [CrossRef]
54. Niu, X.; Liu, Y.; Fang, G.; Huang, C.; Rojas, O.J.; Pan, H. Highly Transparent, Strong, and Flexible Films with Modified Cellulose Nanofiber Bearing UV Shielding Property. *Biomacromolecules* **2018**, *19*, 4565–4575. [CrossRef]
55. Miliani, C.; Monico, L.; Melo, M.J.; Fantacci, S.; Angelin, E.M.; Romani, A.; Janssens, K. Photochemistry of Artists' Dyes and Pigments: Towards Better Understanding and Prevention of Colour Change in Works of Art. *Angew. Chem. Int. Edit.* **2018**, *57*, 7324–7334. [CrossRef]
56. Samain, L.; Gilbert, B.; Grandjean, F.; Long, G.J.; Strivay, D. Redox reactions in Prussian blue containing paint layers as a result of light exposure. *J. Anal. At. Spectrom.* **2013**, *28*, 524. [CrossRef]